Cambridge Centre for Computational Chemical Engineering

University of Cambridge

Department of Chemical Engineering

Emission Control: Simultaneous NO-Soot Reduction

Markus Sander [1] , Abhijeet Raj [1] , Oliver R. Inderwildi [1] , Markus Kraft [1] ,

Sven Kureti [2] and Henning Bockhorn [2]

released: 28 May 2008

[1] Department of Chemical Engineering
University of Cambridge
New Museums Site
Pembroke Street
Cambridge, CB2 3RA
UK
E-mail: mk306@cam.ac.uk

[2] Institut für Technische Chemie
und Polymerchemie
Universität Karlsruhe
76128 Karlsruhe
Germany

c4e

Abstract

In this study the non-catalytic interaction between soot and nitric oxide (NO) is investigated. Recent studies demonstrate that the decomposition of nitric oxide at radical carbon sites on a soot molecule forms surface nitrogen and oxygen. The surface nitrogen can be recombined to gaseous N_2 while the surface oxygen desorbs from the soot molecule as CO. This non-catalytic conversion of gaseous NO into N_2 is investigated using Density Functional Theory (DFT), Transition State Theory and a kinetic Monte-Carlo simulation (kMC) at 560°C on a radical zigzag soot surface. The results are validated against experimental observations. The DFT calculations have been performed with DMoL3 utilizing the HCTH exchange functional. A mechanism for the conversion of NO to N_2 on a zigzag soot surface is explored. The geometries of the intermediate stable species as well as the transition states were optimized to identify the different reaction steps. The vibrational frequencies, geometry, energy, spin population and bond population were computed in these DFT calculations to evaluate the forward and backward reaction rate of each intermediate reaction applying Transition State Theory. A kinetic Monte-Carlo simulation employing the current rates and intermediate species demonstrates feasible mechanisms for the conversion of NO to N_2 on a soot surface. It is also suggested that a portion of NO is trapped on the soot surface. The amount of trapped NO increases during the reaction and blocks the active carbon sites inhibiting further reactions. By combining different theoretical techniques in a multi-scale model, we are for the first time able to describe the conversion of soot in presence of NO accurately.

Contents

1 Introduction

Diesel exhaust contains many harmful substances including soot, NO_x and CO. The removal of these pollutants is hence important for the environment and consequently for human health. The reduction of soot and NO_x has been investigated by many researchers and most of the studies published in this area have investigated the removal of either NO_x or soot from the exhaust gas. Diesel particulate filters are the most favoured exhaust treatment to reduce soot whereas NO_x storage catalysts are preferred to abate NO_x. Twigg summarizes these exhaust-gas aftertreatment techniques in a recent review [29]. The reduction of NO_x has mainly been studied in the presence of catalysts [2, 4, 6, 22], however the direct interaction between soot and NO_x can also remove both substances concertedly. This direct non-catalytic reaction between nitrogen oxide and soot is studied in [1, 10, 23, 26–28, 31]. In most of these studies the hydrogen atoms have been removed from the soot by oxygen to create free radical carbon sites, denoted as C(). NO attaches to two neighboring active carbon sites forming surface nitrogen C(N) and surface oxygen C(O)

$$2C() + NO \rightarrow C(N) + C(O) \text{ or CO}. \tag{1}$$
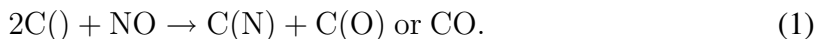
The surface nitrogen C(N) recombines to N_2 as suggested by [7, 8, 10, 23]:

$$C(N) + C(N) \rightarrow N_2 + 2C() \tag{2}$$

$$C(N) + NO \rightarrow N_2 + C(O) \text{ or CO}. \tag{3}$$
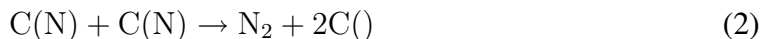
Similar surface decomposition processes are also observed on nobel metal surfaces [16, 17].

There is evidence in the literature that soot is formed of polycyclic aromatic hydrocarbons (PAH) [3, 14, 25]. These PAHs are organized in layers that are stacked together forming a soot molecule as suggested by Transmission Electron Microscopy and X-ray diffraction studies [9]. The surface properties of soot can be studied using a small PAH molecule. This is important as the computational time of DFT calculations depends strongly on the size of the molecule. A first attempt to study the direct soot-NO interaction without catalysts using DFT was made by Kyotani and Tomita [18] but transition states and reaction rates were not reported in this work.

The purpose of this work is to clarify the non-catalytic interaction between soot and molecular nitric oxide. Different reaction pathways proposing the intermediate steps of the reactions (1), (3) and (2) are presented. These two pathways describing the reduction of NO on a zigzag soot surface are studied using DFT calculations, Transition State Theory and kinetic Monte-Carlo simulations. The geometries of the transition states and the stable species were optimized. The energy, the vibrational frequencies, the spin population and the bond population of the geometry optimized species were also computed in these DFT calculations to determine the forward and backward reaction rate of each intermediate reaction applying Transition State Theory. Finally, a kinetic Monte-Carlo simulation at 560°C employing the current rates and intermediate species demonstrates the conversion of NO into N_2 on a soot surface. These results were validated against experimental observations.

2 Calculation Details

A naphthacene molecules with four unsaturated carbon atoms on which the nitric oxide molecule attaches represents the free radical carbon atoms of a soot surface for computational reasons. All the DFT calculations were performed using DMoL3 as included in the Materials Studio software package [11]. The generalized gradient approximation (GGA) corrected HCTH functional [15] was used. This functional has been fitted to a training set of 407 atomic and molecular systems [5]. The double numerical atomic orbital augmented by a polarized function basis set (DNP) that is comparable to the 6-31G** basis set was selected. All the calculations were performed with fine settings for calculation accuracy. The thresholds are: 1×10^{-5} Ha for the maximum energy change, 2×10^{-3} Ha/Å for the maximum force and 5×10^{-3} Å for the maximum displacement. Smearing was turned off for all the calculations except transition state 1: In this calculation 0.004Ha of smearing to the orbital occupation was applied to achieve electronic convergence. The single point energy of species 2 respectively species 3 used to determine the activation energy ΔE_{act} for the reaction from species 2 to species 3 over transition state 1 and vice versa was also calculated with smearing to minimize the error. A geometry optimization was performed to determine the geometry of each stable species and the vibrational frequencies were calculated verifying that there are no imaginary frequencies. Transition states were verified by vibrational analysis. The optimizations were performed for different spin multiplicities. The multiplicity with the lowest energy and a reasonable geometry as well as spin densities was chosen as proposed by Kyotani and Tomita [18]. The bond population analysis was performed using the Mayer calculation method [19], which provides bond orders that are close to the corresponding classical values. The Mulliken spin population analysis [20] was applied to calculate the spin densities. The temperature dependent reaction rates $k(T)$ were calculated with Transition State Theory applying

$$k(T) = \frac{k_B T}{h} \frac{Q^{\neq}}{Q_A Q_B} \exp\left(\frac{-\Delta E_{act}}{k_B T}\right) \tag{4}$$

for bimolecular reactions and

$$k(T) = \frac{k_B T}{h} \frac{Q^{\neq}}{Q_A} \exp\left(\frac{-\Delta E_{act}}{k_B T}\right) \tag{5}$$

for unimolecular reactions. $Q^{\neq}$ is the total partition function of the transition state, Q_A and Q_B the partition function of the the reactants A and B and ΔE_{act} is the activation energy of the reaction. T is the temperature, h Plancks constant and k_B the Boltzmann constant. The total partition function is calculated as the product of the vibrational, translational, rotational and electronic partition functions.

The reaction rates were calculated using Transition State Theory ranging from 20°C to 2700°C in 10°C steps and a linear least-square fitting algorithm was used to fit the rate coefficients A, n and ΔE applying the modified Arrhenius expression:

$$k(T) = A \times T^n \times \exp\left(\frac{-\Delta E}{RT}\right). \tag{6}$$
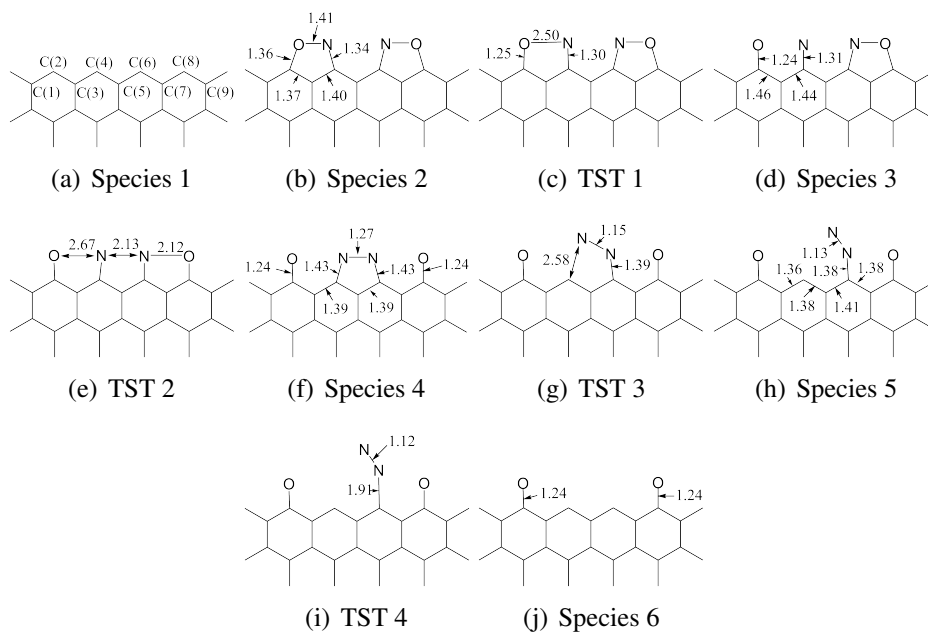
Figure 1: *Stable species and transition states of reaction pathway 1. The numbers indicate the bond length in* Å.

3 DFT calculations

Two different reaction pathways were studied clarifying the intermediate reactions during the reduction of NO on a radical soot surface. Reaction pathway 1 and 2 can be described by the reactions (1) and (3), and (1) and (2) respectively. Detailed information can be found in figure 2 and 4. Both pathways start with a naphthacene molecule with four active sites (Species 1) and two free NO molecules. The Mulliken spin population analysis of the activate carbon atoms is either close to +1 or -1 confirming that there is one unbound electron on each unsaturated carbon atom. The pathways lead from naphthacene(Species 1) and NO to molecular N_2 and oxidized carbon sites C(O) (Species 6 and Species 9). The CO desorption process as proposed in reaction (1) and (3) from the soot surface has been widely discussed in the literature [12, 24, 30, 32] and is therefore not investigated in this study.

In the following section the two reaction pathways are described in detail. The numbering of the C-atoms in the naphthacene molecule is shown in figure 1(a).

Pathway 1:

Figure 1 shows the stable species together with the transition states of reaction pathway 1. The energy surface can be found in figure 2. Table 2 displays the enthalpy of the species in this pathway compared to the enthalpy of the starting point: a naphthacene molecule with four active carbon atoms (species 1) and two free NO molecules. Bond length and bond population details can be found in table 1.

The two nitric oxide molecules attach with the N-O bond axis parallel to the edge of the naphthacene molecule without any reaction barrier on the surface. Two ring structures containing N and O on top of the naphthacene (species 2) are created. This exothermic
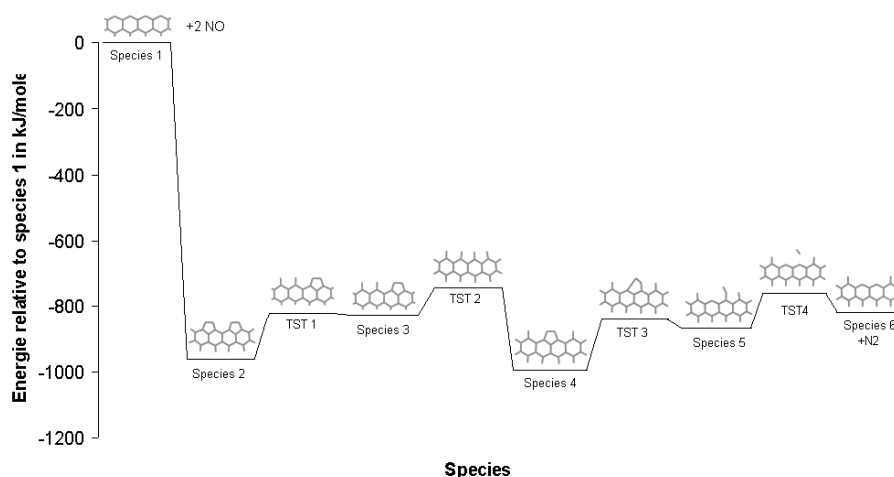
Figure 2: *Energy surface of reaction pathway 1 in* kJ/mol

reaction releases 963.7 kJ/mol and the N-O bond is stretched from 1.15 Å to 1.4 Å. The bond population of the N-O bond diminishes from 2.05 to 1.07 indicating that the new bonds formed to the carbon atoms and the stretching of the bond length reduce the strength of the nitric-oxygen bond significantly. This low bond population facilitates the breakage of the N-O bond. An activation energy of 133.4 kJ/mol is necessary to break the N-O bond (TST 1) and to create species 3. A small smearing of 0.004Ha has been used to achieve convergence for the calculation of transition state 1. The calculation difficulties are caused by the flat energy surface in this region. The energy difference between transition state 1 and stable species 3 is only 2.3 kJ/mol. After the first N-O bond is broken the bond between the oxygen atom and the carbon atom C(1) as well as the bond between the nitrogen atom and the carbon atom C(2) are fortified. The bond population of the nitrogen-carbon bond increases from 1.5 to 1.6 while the oxygen-carbon bond population increases from 1.1 to 1.7. The spin population of the nitrogen atom that is only bound to the carbon atom C(4) is 1.4 indicating that there are unbound electrons. This radical nitrogen atom facilitates the breakage of the bond between the other nitrogen and oxygen atom as it attracts the second nitrogen atom. This second N-O bond is broken with an activation energy of 87.8 kJ/mol (TST 2) and a bond between the two nitrogen atoms is formed (species 4). The bond population of the N-N bond is 1.75. The bond of the nitrogen atoms to the carbon atoms is degraded by the strong N-N bond and the first of the two N-C bond can be broken with an energy of 151.5 kJ/mol (TST 3). The activation energy to break the second bond and to release molecular nitrogen from the structure is 108.5 kJ/mol (TST 4).

Pathway 2:
Figure 3 and figure 4 present the stable species and transition states as well as the energy surface of reaction pathway 2. The bond length and population details are presented in table 5. This pathway is shorter than pathway 1 and only three neighboring active carbon sites are necessary. In order to compare the results of pathway 2 to pathway 1 the same starting configuration has been chosen. In the first reaction step the first NO

Table 1: *Bond length in Å and Mayer bond population for reaction pathway 1.*

| Species	Bond	length in Å	population
Species 1	C(1)-C(2)	1.35	1.55
	C(2)-C(3)	1.40	1.24
	C(3)-C(4)	1.37	1.38
	C(4)-C(5)	1.38	1.31
Species 2	C(1)-C(2)	1.39	1.28
	C(2)-C(3)	1.37	1.26
	C(3)-C(4)	1.40	1.14
	C(4)-C(5)	1.42	1.12
	C(2)-O	1.36	1.06
	N-O	1.41	1.08
	C(4)-N	1.34	1.47
Species 3	C(1)-C(2)	1.45	1.12
	C(2)-C(3)	1.46	1.08
	C(3)-C(4)	1.44	1.11
	C(4)-C(5)	1.45	1.11
	C(2)-O	1.24	1.70
	C(4)-N	1.31	1.61
Species 4	C(3)-C(4)	1.39	1.33
	C(4)-C(5)	1.39	1.19
	C(4)-N	1.43	1.10
	N-N	1.27	1.75
Species 5	C(5)-C(6)	1.41	1.17
	C(6)-C(7)	1.38	1.26
	C(6)-N	1.38	1.02
	N-N	1.32	2.45
Species 6	C(1)-C(2)	1.45	1.10
	C(2)-C(3)	1.47	1.03
	C(3)-C(4)	1.36	1.43
	C(4)-C(5)	1.38	1.29
	C(2)-O	1.24	1.77

molecule chemisorbs with the N-O bond axis parallel to the soot surface forming a 5-member ring (species 7) as in reaction pathway 1, but in contrast to pathway 1 the second NO molecule adsorbs with the oxygen atom down on the radical carbon atom next to the already adsorbed nitrogen atom. A bond between the two nitrogen atoms is formed and both nitrogen-oxygen bonds are broken in the same step (species 8). The activation energy of this reaction is 12.7 kJ/mol (TST 5). The bond populations are close to the values of reaction pathway 1. The activation energy to release the N_2 molecule from the soot surface is 96.3 kJ/mol (TST 6). The N_2 abstraction reaction of reaction pathway 2 needs less energy than the similar reaction of pathway 1 because the enthalpy of species 5 is 9.8kJ/mol less than the enthalpy of Species 8.

Reaction rates:
The forward and backwards reaction rates have been calculated using Transition State
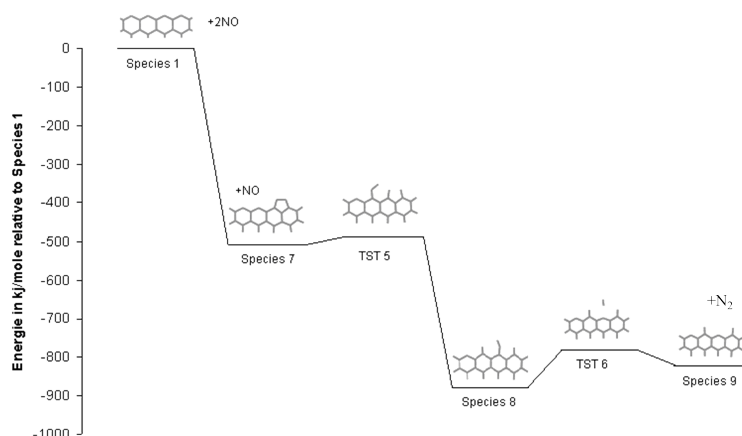
Table 2: *Enthalpy in* kJ/mol *of the species in reaction pathway 1 compared to species 1 and two nitric oxide molecules.*

Structure	ΔH without smearing	ΔH with smearing
Species 1 + 2 NO	0	
Species 2	-963.7	-963.7
TST 1		-830.3
Species 3	-828.3	-832.6
TST 2	-740.5	
Species 4	-994.6	
TST 3	-843.1	
Species 5	-867.0	
TST 4	-758.5	
Species 6	-794.5	

(a) Species 7   (b) TST 5   (c) Species 8   (d) TST 6
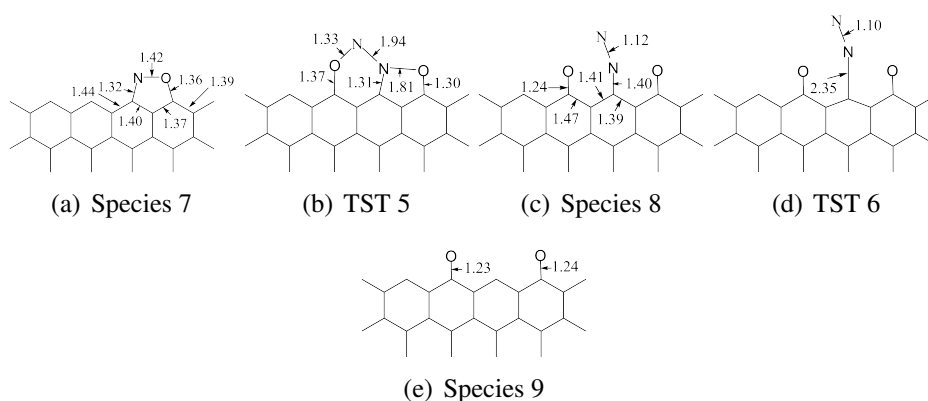
(e) Species 9

Figure 3: *Stable species and transition states of reaction pathway 2. The numbers indicate the bond length in* Å.

Theory and a linear least-square fitting algorithm was used to determine the parameters A, n and ΔE (see equation 6). The reaction rate for the barrier-less NO absorption reaction has not been calculated as variational Transition State Theory is needed to calculate the reaction rate of barrierless reactions. This reaction should be very fast compared to the other rates as indicated by the experiments and therefore the rate can be neglected compared to the other rates. The forward and backward reaction rate for the reaction from species 2 to species 3 has been calculated with 0.004 Ha of smearing for the transition state. In order to minimize the error the energy of the reactants of this one reaction were also calculated with the same smearing to reduce the error in the activation energy. All the other reaction rates were calculated without smearing. The Arrhenius parameters for pathway 1 can be found in table 4 and for pathway 2 in table 6.

Figure 4: *Energy surface of reaction pathway 2 in* $\mathrm{kJ/mol}$

Table 3: *Enthalpy of the species in reaction pathway 2 compared to species 1 and two nitric oxide molecules.*

| Structure	ΔH in $\mathrm{kJ/mol}$
Species 1 + 2 NO	0
Species 7 + NO	-503.8
TST 5 + NO	-491.1
Species 8	-876.8
TST 6	-780.5
Species 4	-818.3

4   Experimental Work

Detailed information about the experimental study can be found in [22]. In this paper only the important parts that consider the direct soot NO interaction are summarized.

Setup:
The examinations are done under isothermal conditions at 560°C. In the first stage the active carbon sites on the soot surface have been prepared by oxidizing the soot with O_2 (5.0 vol.% O_2, 95 vol.% Ar) until a defined conversion level of 75% has been reached. Afterwards in the second stage the soot is flushed with Ar and the temperature is increased to 715°C to allow the CO molecules to desorb. These two steps prepare a soot surface with activated carbon atoms. This soot structure with the active carbon sites is exposed in the third stage to a gas mixture of 500 ppm NO in Ar. To analyze the composition of the soot after the NO exposure a Temperature Programmed Oxidation (TPO) with 5.0- vol % O_2 in Ar up to 715°C at a rate of 10°C/min is performed (fourth stage). Figure 5 represents the stages three and four.

Table 4: *Arrhenius parameters for reaction pathway 1. A in* $(1/\mathrm{s})$ *for unimolecular reactions and* $\mathrm{cm}^3/(\mathrm{mol}\cdot\mathrm{s})$ *for bimolecular reactions,* ΔE *in* $\mathrm{kJ/mol}$. *Bimolecular reactions are marked with an asterisk.*

Reaction	A	n	ΔE
$2 \to 3$	2.2×10^{13}	0.34	127.3
$3 \to 2$	1.8×10^{12}	0.10	1.5
$3 \to 4$	1.8×10^{12}	0.44	78.7
$4 \to 3$	1.0×10^{12}	0.45	244.0
$4 \to 5$	9.3×10^{12}	0.23	148.1
$5 \to 4$	3.2×10^{12}	0.07	23.6
$5 \to 6$	2.0×10^{13}	0.11	108.6
$6 \to 5$	1.7×10^{3}	2.51	38.9*
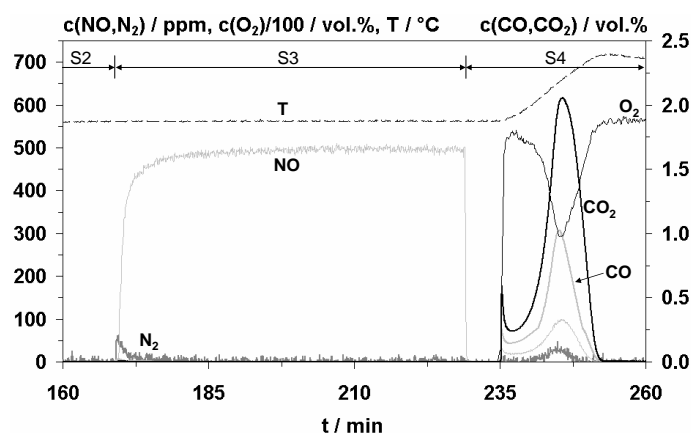
Figure 5: *Concentration of* CO, CO_2, O_2, NO *and* N_2 *and the temperature as a function of time.* Si *represents the* i^{th} *stage in soot oxidation process.* $S1$ *involving partial oxidation of soot in* O_2-Ar *environment is not shown here.*

Results:

The experimental results are presented in figure 5. To clarify the experimental observations directly after the NO exposure a enlarged graph can be found in figure 6. This graph shows that the NO molecules adsorb on the active carbon sites instantaneously. NO does not remain in the surrounding gas in the first 20 seconds of NO exposure. The amount of NO in the surrounding gas increases rapidly after the active carbon sites are saturated. N_2 and a small amount of CO is formed directly after the NO exposure. The amount of N_2 released from the soot is less than the amount of NO consumed suggesting there is a portion of NO trapped on the soot surface. The reaction stops and a significant amount of nitric oxide that ranges from 40 to 63 % remains on the soot surface. The TPO after the NO exposure oxidizes the soot entirely and releases N_2 as well as NO, CO and CO_2 confirming that some NO molecules have been bound to the soot molecule.

**Table 5:** *Bond length in Å and Mayer bond population for reaction pathway 2.*

Species	Bond	length in Å	population
Species 7	C(5)-C(6)	1.44	1.05
	C(6)-C(7)	1.41	1.15
	C(7)-C(8)	1.37	1.26
	C(8)-C(9)	1.40	1.27
	C(6)-N	1.32	1.54
	N-O	1.41	1.06
	C(9)-O	1.36	1.08
Species 8	C(3)-C(4)	1.47	1.05
	C(4)-C(5)	1.47	1.07
	C(4)-O	1.24	1.76
	C(5)-C(6)	1.40	1.24
	C(6)-C(7)	1.39	1.25
	C(6)-N	1.40	0.98
	N-N	1.12	2.52
Species 11	C(3)-C(4)	1.49	1.01
	C(4)-C(5)	1.46	1.05
	C(7)-C(8)	1.46	1.05
	C(8)-C(9)	1.46	1.09
	C(4)-O	1.23	1.83
	C(8)-O	1.24	1.77

Table 6: *Arrhenius parameters for reaction pathway 2. A in* $(1/\mathrm{s})$ *for unimolecular reactions and* $\mathrm{cm}^3/(\mathrm{mol} \cdot \mathrm{s})$ *for bimolecular reactions,* ΔE *in* $(\mathrm{kJ/mol})$. *Bimolecular reactions are marked with an asterisk.*

Reaction	A	n	ΔE
Species7 → Species8	3.2×10^2	2.62	11.0*
Species8 → Species7	6.7×10^{11}	0.27	379.9
Species8 → Species9	3.6×10^{13}	0.4	89.3
Species9 → Species8	2.5×10^3	2.65	35.3*

5 KMC simulations

The present study utilizes a detailed Monte-Carlo model, named as Kinetic Monte Carlo–Aromatic Site (KMC-ARS) model, to study the oxidation of PAHs present in soot particles in a nitric oxide–Argon (NO-Ar) environment. The KMC-ARS model is based on the processes involved in the two pathways for soot oxidation described above, along with some soot oxidation processes taken from [12, 30] as shown in table 7. These PAH processes are allowed to take place on a substrate PAH molecule. In this work a substrate rich in zig-zag site was chosen (figure 7(a)) as most of the processes listed in table 7 involve such sites. After a process takes place on the substrate the KMC-ARS model determines the resulting structure of the substrate molecule based on the positions of C, N and O atoms and relative positions of the reactive sites. Full description of this model can be obtained in [21]. This work involves the simulation of oxidation of a PAH molecule by
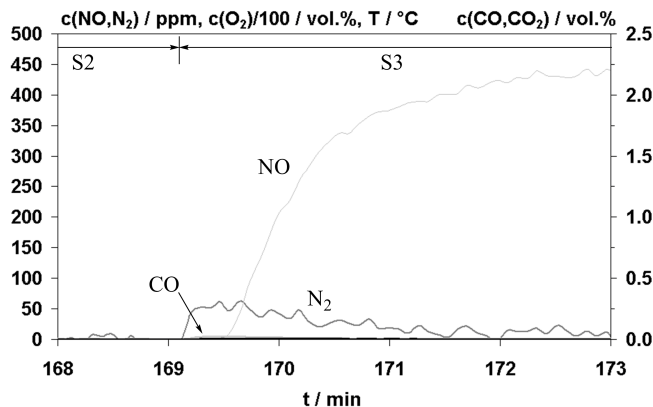
Figure 6: *Concentration of* CO, CO_2, O_2, NO *and* N_2 *and the temperature as a function of time shortly before and after the* NO *exposure.*
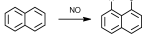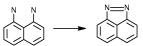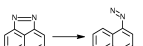

(a)   (b)
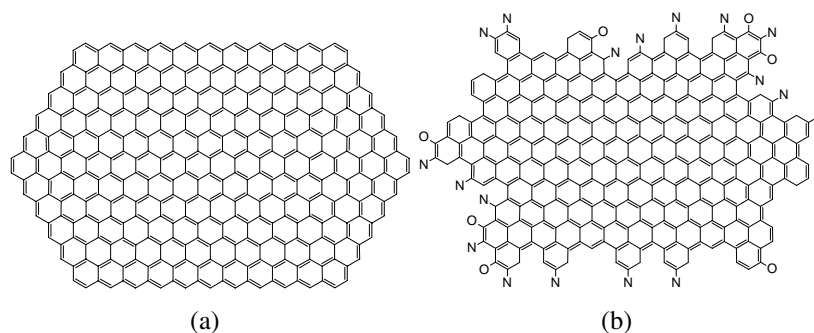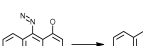
Figure 7: *(a) An example PAH substrate. (b) An example computed PAH obtained aftere a simulation of 0.15 s. No further reaction can take place on this molecule with the present reaction pathway.*
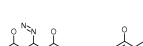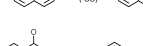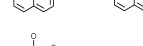
NO in a gas-phase environment of NO and Ar studied in this work (see section 4). The substrate is assumed to be at the same temperature as the gas-phase environment which is equal to 560°C. Pressure and NO concentration are taken to be 1 atm and 500 ppm respectively. These conditions are assumed to remain unchanged throughout the simulation. The stochastic algorithm developed to track the structure of PAHs after each reaction step is detailed in [21] and is briefly reviewed here. The process of PAH oxidation by NO is modelled as a Markovian sequence of reaction events [13]. The outcome of this model depends on the concentration of reacting species, the rates of the possible reaction events and the probability of a reaction to be chosen. The rates for the processes listed in table 7 are calculated as:

$$R_i = k_i \times C_s \times N_{site}, \quad i = 1, 2 \ldots I$$

where I is the number of processes in table 7, C_s is the concentration of chemical species involved in the bimolecular reactions and N_{site} is the number of reactive sites on the PAH

12

Table 7: *PAH processes. The units of T and R are* K *and* kJ/(mol.K) *respectively. For reaction 1, rate has been assumed to be infinitely fast. Rate constants for reactions 8–10 has been taken from [12, 30].*

No.	Process	Rate constant, k
1		infinitely fast
2		$2.2 \times 10^{13} T^{0.34} e^{\frac{-127.3}{RT}}$
3		$1.8 \times 10^{12} T^{0.44} e^{\frac{-78.7}{RT}}$
4		$9.3 \times 10^{12} T^{0.23} e^{\frac{-148.1}{RT}}$
5		$2.0 \times 10^{13} T^{0.11} e^{\frac{-108.6}{RT}}$
6		$3.2 \times 10^{2} T^{2.62} e^{\frac{-11}{RT}}$
7		$3.6 \times 10^{13} T^{0.4} e^{\frac{-89.3}{RT}}$
8		$7.4 \times 10^{11} e^{\frac{-92.3}{RT}}$
9		$7.4 \times 10^{11} e^{\frac{-92.3}{RT}}$
10		$7.4 \times 10^{11} e^{\frac{-92.3}{RT}}$

molecule involved in the process i. At time t, an exponentially distributed waiting time for a reaction to take place τ with parameter λ is calculated where λ is the sum of all the process rates:

$$\lambda = \sum_{i=1}^{I} R_i$$

$t = t + \tau$ gives the time for the next reaction. A reaction is chosen based on the probability calculated using its reaction rate. A site of correct type is chosen uniformly assuming all sites to be equally probable. The substrate structure is then updated based on the chosen process and the above procedure is repeated for the desired simulation time. The results obtained from the simulations are discussed in the next section.

KMC Results:
As mentioned in section 4 the complete oxidation of soot takes place in four stages: partial oxidation of soot in an O_2-Ar environment; removal of CO in Ar environment to create radical sites on soot; exposure of soot particles with radical sites to NO-Ar environment where NO molecules get deposited on soot surface with some removal of N_2 and CO

(partial oxidation); further oxidation of soot in an O_2-Ar environment. In this work only the third stage of this oxidation process has been simulated assuming the substrate to be full of radical sites. This is because detailed reaction pathway showing the interaction of O_2 with PAHs were not considered in this work and will be investigated in the a future study. The reaction rate of reaction 1 (table 7) has been assumed to be infinitely fast. This signifies that the substrate would be uniformly populated with NO molecules in the beginning of the simulations. Figure 7(b) shows an example computed PAH molecule obtained after a real time simulation of 0.15 s in a NO-Ar environment. It was noticed that the addition of NO on soot surface subsequently leads to the removal of C atoms in the form of CO or HCCO through reactions 8–10 (table 7). Figure 8 shows the number of reaction events normalized with the number of C atoms on the substrate molecule after a real time simulation of 0.15 s, averaged over 100 simulation runs. It can be noticed in
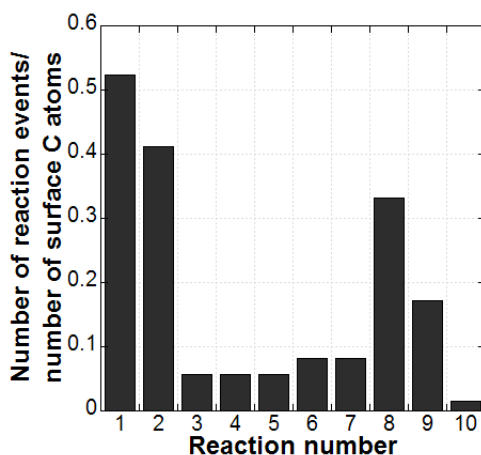
Figure 8: *Average number of reaction events normalised with the number of surface carbon atoms on the substrate* PAH *after a real time simulation of 0.15 s. The reactions corresponding to the reaction numbers (on x-axis) can be obtained from table 7.*

this figure that reaction 5 involved in pathway 1 takes place less frequently than reaction 7 involved in pathway 2. This implies that pathway 2 contributes more to the formation of N_2 molecules than pathway 1 as pathway 1 requires the presence of two adjacent N atoms and this may not occur very frequently. With the progress of the reaction the resulting PAH structure develops bay-type structures prohibiting further addition of NO on PAHs with the present reaction pathway. Additionally, it can be noticed in figure 7(b) that there are a number of N and O atoms on PAH edges which cannot be removed. Therefore no further oxidation of PAHs with NO molecules can take place after some time. These results are qualitatively in agreement with the experimental observation. Experimentally observed concentration profiles of NO, CO and N_2 in stage 3 (see figure 5) show that addition of NO on soot surface along with removal of N_2 and CO takes place in the beginning (before 173 min). Thereafter the concentration of NO becomes almost constant indicating negligible oxidation of soot particles by NO. It is difficult to make any quantitative comparison as there might be many other reactions taking place on PAH edges like

addition of NO on bay sites and oxidation of phenalene-like structures (see figure 7(b)) during the oxidation processes.

6 Conclusion

Two different reaction pathways leading from a soot molecule with a surface containing radical carbon atoms and nitric oxide in the surrounding gas to oxidized soot and molecular N_2 were explored using quantum mechanical calculations. The computed reaction rates and species were used in a kinetic Monte-Carlo simulation. The theoretical results are consistent with the experimental observations. Figure 8 displays that reaction pathway 2 (reaction number 6,7) is slightly preferred against pathway 1 (reaction number 3,4,5) as only three free radical sites are needed. The different reaction steps in each pathway occur the same number of times demonstrating that once the nitric oxide molecules are bound to the soot surface and the current alignment allows further reactions N_2 is formed quickly. This is consistent with the experimental observations (see figure 6) where the NO exposure in the third experimental stage leads to an immediate N_2 production. Hence, the kMC results based on a DFT derived reaction mechanism presented herein are able to describe experimental observations.

Figure 7(b) clarifies the reasons why a portion of NO remains trapped on the soot surface. The calculations demonstrate that the alignment of the nitric oxide molecules is crucial in the pathways. Two NO molecules attached to the surface in the wrong direction (N-O-N-O) block the active carbon sites and remain trapped on the soot molecule as seen in the left down edge of the soot molecule in figure 7(b). The vacancies created by CO desorption processes inhibit subsequent decomposition of NO molecules on the surface. Nevertheless NO can adsorb on the vacancies as found by Kyotani and Tomita [18] but this leads to very stable structures and hence further decomposition is unlikely at 560°C. The importance of the correct alignment, the holes created by CO desorption processes as well as trapped oxygen and nitrogen atoms on the soot surface explain the cease of the reaction and the low amount of N_2 and CO formed in the third experimental stage. There are also other reactions and pathways between soot and NO possible, however, as the influence of these reaction is most likely negligible our theoretical investigations match the experimental data.

At the moment we consider only the forward reaction processes in our kinetic Monte-Carlo simulations, but it has been demonstrated that the initial adsorption position and geometry of the nitric oxide molecules on the soot surface is the crucial part of the reaction. The desorption of NO from the soot surface is negligible as the activation energy is much higher than the dissociation energy. This is confirmed by experiments where NO is not released from the surface before increasing the temperature significantly. As the reaction rate is mainly determined by the sterics of the adsorption process, the backwards reactions most likely have only a minor effect. Therefore we can summarize that our reaction pathways and KMC simulations describe qualitatively the experimental observations. This study represents the first comprehensive theoretical investigation of the reaction mechanism of the non-catalytic soot reduction by NO. A combination of a mechanistic DFT study and a kMC study based hereon enabled a qualitative description of the experimental results of the soot reduction by NO. In the future we will add the backwards

reactions to the KMC simulations as well as some other reactions on different site geometries and try to explain the experimental findings in the fourth experimental stage at higher temperatures and in an oxygen rich environment.

Acknowledgements

References

[1] I. Aarna and E. M. Suuberg. A review of the kinetics of the nitric oxide-carbon reaction. *Fuel*, 76:475–491, 1997. doi:10.1016/S0016-2361(96)00212-8.

[2] P. Balle, H. Bockhorn, B. Geiger, N. Jan, S. Kureti, D. Reichert, and T. Schroeder. Study on the mechanism of the catalytic conversion of NO_x and soot into N_2 and CO_2 on Fe_2O_3 in diesel exhaust. *Chem. Eng. Process.*, 45:1065, 2006. doi:10.1007/s11244-007-0192-0.

[3] M. Balthasar and M. Kraft. A stochastic approach to solve the particle size distribution function of soot particles in laminar premixed flames. *Combust. Flame*, 133: 289–298, 2003. doi:10.1016/S0010-2180(03)00003-8.

[4] H. Bockhorn, S. Kureti, and D. Reichert. Study on the mechanism of the catalytic conversion of NO_x and soot into N_2 and CO_2 on Fe_2O_3 in diesel exhaust. *Topics in Catalysis*, 42:283–286, 2007. doi:10.1007/s11244-007-0192-0.

[5] A. D. Boese and N. C. Handy. A new parametrization of exchangecorrelation generalized gradient approximation functionals. *J. Chem. Phys.*, 114:5497, 2001. doi:10.1063/1.1347371.

[6] S. A. Carabineiro, F. B. Fernandes, A. M. Ramos, J. Vital, and I. F. Silva. Vanadium as a catalyst for NO, N_2O and CO_2 reaction with activated carbon. *Catalysis Today*, 57:305–312, 2000. doi:10.1016/S0920-5861(99)00341-7.

[7] P. Chambrion, H. Orikasa, T. Kyotani, and A. Tomita. A study of the C—NO reaction by using isotopically labelled C and NO. *Fuel*, 76:493–498, 1997. doi:10.1016/S0016-2361(96)00224-4.

[8] P. Chambrion, T. Kyotani, and A. Tomita. Role of N-containing surface species on NO reduction by carbon. *Energy Fuels*, 12:416–421, 1998. doi:10.1021/ef970182r.

[9] H. X. Chen and R. A. Dobbins. Crystallogenesis of Particles Formed in Hydrocarbon Combustion. *Combust. Sci. Technol.*, 159, 2000.

[10] G. De Soete. Heterogeneous N_2O and NO formation from bound nitrogen atoms during coal char combustion. *Proc. Combust. Inst.*, pages 1257–1264, 1990.

[11] B. Delly. DMol is a density functional theory program distributed by Accelrys Inc. 2006. *J. Chem. Phys.*, 92:508, 1990.

[12] P. Frank., J. Herzler, T. Just, and C. Wahl. High-temperature reactions of phenyl oxidation. *Proc. Combust. Inst.*, 25:833–840, 1994.

[13] M. Frenklach. On surface growth mechanism of soot particles. *Proc. Combust. Inst.*, 26:2285–2293, 1996. doi:10.1016/S0082-0784(96)80056-7.

[14] M. Frenklach. Method of moments with interpolative closure. *Chem. Eng. Sci*, 57: 2229–2239, 2002. doi:10.1016/S0009-2509(02)00113-6.

[15] F. A. Hambrecht, A. J. Cohem, A. J. Tozer, and N. C. Handy. Development and assessment of new exchange-correlation functionals. *J. Chem. Phys.*, 109:6264, 1998. doi:10.1063/1.477267.

[16] O. R. Inderwildi, S. J. Jenkins, and D. A. King. An unexpected pathway for the catalytic oxidation of methylidyne on Rh{111} as a route to syngas. *J. AM. CHEM. SOC.*, 129:1751–1759, 2007. doi:10.1021/ja067722w.

[17] O. R. Inderwildi, S. J. Jenkins, and D. A. King. Dynamic interplay between diffusion and reaction: Nitrogen recombination on Rh{211} in car exhaust catalysis. *J. AM. CHEM. SOC.*, 130:2213–2220, 2008. doi:10.1021/ja0754913.

[18] T. Kyotani and A. Tomita. Analysis of the reaction of carbon with NO/N_2O using ab initio molecular orbital theory. *J. Phys. Chem. B*, 103:3434–3441, 1999. doi:10.1021/jp9845928.

[19] I. Mayer. Bond orders and valences from ab initio wave functions. *Int. J. Quantum Chem*, 29:477–483, 1986.

[20] R. Mulliken. Electronic population analysis on LCAO-MO molecular wave functions. i. *J. Chem. Phys*, 23:1833–1846, 1955. doi:10.1063/1.1740588.

[21] A. Raj, M. S. Celnik, R. I. A. Patterson, R. H. West, and M. Kraft. A statistical approach to develop a detailed soot growth model using pah characteristics. Technical Report 52, c4e Preprint-Series, Cambridge, 2007. URL http://como.cheng.cam.ac.uk.

[22] D. Reichert, H. Bockhorn, and S. Kureti. Study of the reaction of NO_x and soot on Fe_2O_3 catalyst in excess of O_2. *Applied catalysis B*, 80:248–259, 2008. doi:10.1016/j.apcatb.2007.11.024.

[23] J. Rodriguez-Mirasol, A. Oomsa, J. Pelsa, F. Kapteijna, and J. Moulijna. NO and N_2O decomposition over coal char at fluidized-bed combustion conditions. *Combustion and Flame*, 99:499–507, 1994. doi:10.1016/0010-2180(94)90042-6.

[24] K. Sendt and B. S. Haynes. Density functional study of the chemisorption of O_2 on the zig-zag surface of graphite. *Combustion and Flame*, 143:629–643, 2005. doi:10.1016/j.combustflame.2005.08.026.

[25] J. Singh, R. I. A. Patterson, M. Kraft, and H. Wang. Numerical simulation and sensitivity analysis of detailed soot particle size distribution in laminar premixed ethylene flames. *Combust. Flame*, 145:117–127, 2006. doi:10.1016/j.combustflame.2005.11.003.

[26] T. Suzuki, T. Kyotani, and A. Tomita. Study on the carbon-nitric oxide reaction in the presence of oxygen. *Ind. Eng. Chem. Res.*, 33:2840–2845, 1994. doi:10.1021/ie00035a038.

[27] H. Teng, E. Suuberg, and J. Calo. Studies on the reduction of nitric oxide by carbon: the nitric oxide-carbon gasification reaction. *Energy Fuels*, 6:398–406, 1992. doi:10.1021/ef00034a008.

[28] K. Thomas. The release of nitrogen oxides during char combustion. *Fuel*, 76:457–473, 1997. doi:10.1016/S0016-2361(97)00008-2.

[29] M. Twigg. Progress and future challenges in controlling automotive exhaust gas emissions. *Appl. Catal. B.*, 20:2, 2007. doi:10.1016/j.apcatb.2006.02.029.

[30] H. Wang and M. Frenklach. A detailed kinetic modeling study of aromatic formation in laminar premixed acetylene and ethylene flames. *Combust. Flame*, 110:173–221, 1997. doi:10.1016/S0010-2180(97)00068-0.

[31] H. Yamashita, A. Tomita, A.Yamada, T.Kyotani, and L. R. Radovic. Influence of char surface chemistry on the reduction of nitric oxide with chars. *Energy and Fuels*, 7:85, 1993. doi:10.1021/ef00037a014.

[32] Z. H. Zhu and G. Q. Lu. New insights into NO-carbon and N_2O-carbon reactions from quantum mechanical calculations. *Energy and Fuels*, 17:1057–1061, 2003. doi:10.1021/ef0202079.